Soil Genesis and Mineral Transformation Across an Environmental Gradient on Andesitic Lahar

Craig Rasmussen*
Soil, Water, and Environmental Science Dep.
Univ. of Arizona
Shantz Bldg. no. 38
1177 E. Fourth St.
P.O. Box 210038
Tucson, AZ 85721

Nobuhiko Matsuyama
Faculty of Agric. and Life Science
Hirosaki Univ.
3 Bunkyo
Hirosaki
Aomori 036-8561
Japan

Randy A. Dahlgren
Randal J. Southard
Neil Brauer
Land, Air, and Water Resources
Univ. of California-Davis
One Shields Ave.
Davis, CA 95616

Soils derived from andesite are regionally important in the western USA, and expression of andic soil properties may be directly related to climate. The objective of this research was to quantify mineral transformation on andesitic lahar across an environmental gradient on the western slope of the Sierra Nevada of California. We hypothesized that the dominance of short-range-order (SRO) materials would increase with increasing elevation as precipitation increased and temperatures decreased. Seven pedons were sampled across an elevation gradient (150–2800 m) having large variations in mean annual soil temperature (3–17°C) and mean annual precipitation (45–150 cm). The soil mineral assemblage was characterized by x-ray diffraction, selective dissolution, total elemental analysis, and microprobe analysis. Weathering and soil development displayed maxima in the zone just below the permanent winter snowline (~1590 m), with a sharp decrease at higher elevations. Rainfall-dominated soils at lower elevations had a clay fraction dominated by kaolin. In the snowfall-dominated zone, SRO (allophane and imogolite) dominated the clay fraction, except for the soils in the cryic soil temperature regime, where interlayered 2:1 layer silicates dominated. The 2:1 mineral is probably inherited, based on the presence of a chlorite-like mineral in the andesite parent material. With increasing elevation, soil development followed the order Mollisols → Alfisols → Ultisols → Andisols → Inceptisols. Weathering, mineralogical transformations and soil development are limited by water availability at low elevations, whereas low soil temperature is the major limitation at high elevations.

Abbreviations: AL-7, alpine biome; Al_d, citrate–dithionite-extractable aluminum; Al_o, oxalate-extractable aluminum; Al_p, pyrophospate-extractable aluminum; BO-1, blue oak biome; Fe_d, citrate–dithionite extractable iron; Fe_o, oxalate-extractable iron; PO-2, pine–oak biome; PP-3, ponderosa pine biome; RF-5, red fir biome; SA-6, subalpine biome; Si_o, oxalate-extractable silicon; SRO, short-range ordered; WF-4, white fir biome; XRD, x-ray diffraction.

Soils derived from andesite are regionally important in the volcanically active western USA, comprising a significant portion of the mountainous areas of Washington, Oregon, Idaho and California (Soil Survey Staff, 1999). Soils derived from andesite often exhibit andic properties, such as low bulk density, variable charge, high water retention, high phosphate retention, and high organic C content (Shoji et al., 1993). These distinctive properties are primarily attributed to a dominance of noncrystalline and SRO weathering products, including allophane, imogolite, ferrihydrite, and Al–humus complexes (Dahlgren et al., 2004). Expression of these characteristics depends on the degree of soil development, and various weathering scenarios have been proposed to explain mineral formation and transformation within volcanic-ash-derived soils (Fieldes, 1955; Parfitt et al., 1983; Shoji et al., 1993; Zehetner et al., 2003).

Fieldes (1955) proposed that weathering of volcanic parent materials containing glass and ash components involves the rapid dissolution of volcanic glass and oversaturation of soil solution with respect to metastable SRO materials. Preferential precipitation of SRO materials occurs through nucleation of a more soluble phase (i.e., SRO materials) that is kinetically favored over that of a less soluble phase (i.e., crystalline mineral) due to the lower solid–solution interfacial tension of the more soluble phase (Stumm, 1992). Thus, nucleation of a noncrystalline phase will occur at a lower degree of supersaturation, resulting in a higher nucleation rate relative to crystalline minerals. With time, crystalline minerals form at the expense of their metastable SRO precursors. The "aging" or "Ostwald ripening" process (i.e., transformation of SRO materials to crystalline phases via dissolution and reprecipitation) typically occurs over relatively long time periods due to the small differences in free energy between the two phases. This sequence of kinetically controlled precipitation of SRO materials and subsequent transformation to more thermodynamically stable kaolin minerals has been proposed to explain mineral assemblage variation across numerous chronosequences (time spans of 10^1–10^5 yr) on volcanic materials (Kirkman, 1980; Naidu et al., 1987; Wada, 1989; Bakker et al., 1996; Chadwick and Chorover, 2001).

Climatic conditions and their effects on degree of leaching and soil solution chemistry also play an important role in volcanic material weathering pathways and secondary mineral neogenesis. Volcanic materials may weather directly to SRO materials or kaolins, depending on the amount of rainfall and solution silica activity (Parfitt et al., 1983). Indeed, some studies have shown that crystalline clays, such as halloysite, form initially without a SRO precursor in weathering systems that exhibit high solution silica activity (McIntosh, 1979; Singleton

Soil Sci. Soc. Am. J. 71:225-237
doi:10.2136/sssaj2006.0100
Received 3 Mar. 2006.
*Corresponding author (crasmuss@ag.arizona.edu).

et al., 1989). Low rainfall or leaching promote high solution silica activity, facilitating halloysite formation, whereas high precipitation or leaching promote low silica activity, favoring SRO material formation (Parfitt et al., 1983). Coupled with precipitation, temperature also plays a role in the formation of SRO materials or crystalline minerals, with crystallization promoted as the soil climate becomes warmer and drier (Talibudeen, 1981; Schwertmann, 1985). Short-range ordered materials are more persistent under cool soil conditions because crystallization is hindered by low input of thermal energy. Seasonal soil desiccation has also been shown to enhance transformation of noncrystalline and SRO materials to crystalline minerals (Quantin, 1992). Climate appears to control both the initial weathering products (SRO materials or kaolin minerals) and the potential rate at which initial weathering products undergo transformation to more stable phases.

Allophane and andic soil properties form relatively rapidly on andesitic parent materials in the mesic soil temperature and xeric moisture regimes of California, e.g., on andesitic mudflows near Mt. Shasta, California, soils were classified as Haploxerands with detectable concentrations of allophane (25–50 g kg^{-1}) after 600 yr of weathering (Lilienfein et al., 2003, 2004). In contrast, early-Holocene- to late-Pleistocene-aged soils on andesitic mudflows in the Sierra Nevada of California demonstrated a clay mineral assemblage dominated by kaolinite, halloysite, and gibbsite (Southard and Southard, 1987, 1989). The dominance of the clay fraction by allophane in young soils relative to older, highly weathered soils dominated by crystalline kaolin minerals is similar to the mineral assemblage progression noted in other chronosequence studies, and suggests a Fieldes (1955) type sequence as noted above.

Hendricks and Whittig (1968a, 1968b) observed changes in primary mineral transformation products across a sequence of weakly to highly weathered andesitic saprolite in a Haplohumult near Mt. Shasta. Weakly weathered saprolite demonstrated a rapid loss of silica and formation of SRO materials, whereas highly weathered saprolites were dominated by a mixture of SRO and kaolin minerals. It was unclear, however, whether the formation of crystalline minerals at later stages of weathering was due to transformation of SRO precursors or to changes in solution chemistry promoting kaolin formation. In a similar system, Takahashi et al. (1993, 2001) suggested allophane as a metastable precursor to halloysite in young volcanic materials. Further, these researchers and others (Southard and Southard, 1987, 1989) found that surface soil horizons demonstrated a transformation of hydrated halloysite (1.0 nm) to dehydrated halloysite (0.7 nm) or recrystallization to kaolinite, and continued desiliciation to gibbsite. These studies all involved soils with a xeric and mesic soil climate regime and suggest a progression from SRO material → halloysite (1.0 nm) → halloysite (0.7 nm) or kaolinite → gibbsite with continued weathering, dehydration, and desilication. In comparison, soil mineral assemblages across a large environmental gradient on basaltic and andesitic parent materials near Lassen Peak, California, suggest solution silica activity control of secondary mineral formation (Parfitt et al., 1983), with smectite as the dominant mineral under hot, dry conditions, transitioning to dominance by halloysite and then SRO materials under progressively cooler and wetter conditions (Alexander et al., 1993). To date there are no detailed studies documenting changes in soil mineral assemblage across large environmental gradients on andesitic parent materials in the dominantly xeric soil moisture regime of California.

Soils derived from andesite commonly contain 2:1 phyllosilicates in addition to SRO materials and kaolins, but the genesis of these 2:1 minerals is not entirely clear. Their origin has been attributed to a number of processes including: (i) hydrothermal alteration of primary minerals before and during eruption, with subsequent deposition of altered lithic fragments in volcanic ejecta; (ii) in situ weathering from pyroxenes, amphiboles, chlorites, and micas; (iii) alteration of metastable SRO phases with increased weathering; (iv) solid-state transformation of volcanic glass; (v) and eolian inputs (Shoji et al., 1993; Dahlgren et al., 1997b; Nieuwenhuyse and van Breemen, 1997; Chorover et al., 1999; Zehetner et al., 2003). An abundance of 2:1 minerals may inhibit allophane formation through competition for available Al, the so-called "antiallophanic" effect (Shoji et al., 1993; Dahlgren et al., 1997b), analogous to the "antigibbsite" effect proposed by Jackson (1963).

We have expanded on several previous studies in the semiarid, xeric soil moisture regimes of California and the Pacific Northwest (Hendricks and Whittig, 1968a, 1968b; Southard and Southard, 1987; 1989; Dahlgren and Ugolini, 1989; Takahashi et al., 1993, 2001; Lilienfein et al., 2003) to assess mineralogical transformations in andesite across a wide environmental gradient. The objective of this research was to study soil genesis and mineral transformation in an andestic lahar from xeric-thermic to cryic-udic conditions along the western slope of the Sierra Nevada of California. Specifically, we examined temperature and precipitation as the primary factors controlling the distribution of SRO materials and crystalline minerals.

MATERIALS AND METHODS

Environmental Setting

A series of well-drained soils was examined across an elevation gradient (between 150 and 2800 m) on the western slope of the Sierra Nevada in California between 121°13′W and 119°58′W longitude at 38°52′N latitude. The transect spans a broad environmental gradient, with large variation in mean annual soil temperature (3–17°C), mean annual precipitation (45–150 cm) and vegetation (Table 1). With increasing elevation, mean annual soil temperature decreases and mean annual precipitation increases, with the current-day permanent winter snowline occurring near 1590 m (California Department of Water Resources, 1952–1962). All sites are characterized by a Mediterranean climate with warm to hot, dry summers and cool to cold, wet winters. Soil moisture regimes are predominantly xeric, although the high-elevation zone may remain sufficiently moist due to late melting of the snowpack and summer thunderstorm activity to be classified as udic. Soil temperature regime ranges from thermic to cryic with increasing elevation.

Soils were sampled from seven sites across the environmental gradient, with each site named by biome or the dominant overstory vegetation (Table 1). Vegetation progresses from blue oak (*Quercus douglasii* Hook. & Arn.) dominated oak woodlands at low elevation through ponderosa pine (*Pinus ponderosa* C. Lawson), white fir [*Abies concolor* (Gordon & Glend.) Lindl. ex Hildebr.], and red fir (*Abies magnifica* A. Murray) mixed conifer systems at mid elevations, to subalpine mixed conifer and alpine grassland ecosystems at high elevation. Sample sites will be referred to by their abbreviated biome name in combination with

Table 1. Site characteristcs for soils derived from andesite along an elevation and climate gradient in the Sierra Nevada of California.

Mapped soil series	Biome†	Biome ID	Dominant vegetation	Soil taxonomy‡	Elevation	MAT§	MAP§	Precip.§
					m	ºC	cm	
Top¶	Alpine	AL-7	mixed grasses and herbs	loamy-skeletal, mixed, superactive Humic Lithic Dystrocryept	2700	3.0	152	snow
Nobu¶	Subalpine	SA-6	*Abies magnifica, Pinus jeffreyi, P. contorta*	loamy-skeletal, mixed, superactive Vitrandic Dystrocryept	2450	4.5	140	snow
Waca	Red fir	RF-5	*A. magnifica*	medial-skeletal, amorphic, frigid Humic Vitrixerand	2150	6.0	135	snow
McCarthy	White fir	WF-4	*Abies concolor, P. ponderosa, Calocedrus decurrens*	medial-skeletal, amorphic, mesic Humic Haploxerand	1700	8.5	140	snow
Aiken	Ponderosa pine	PP-3	*P. ponderosa, C. decurrens, P. lambertiana, Pseudotsuga menziesii*	fine, parasesquic, mesic Andic Palehumult	1150	11.5	125	rain
Supan	Pine–oak	PO-2	*Quercus douglasii, P. sabiniana*	clayey-skeletal, mixed, active, mesic Ultic Haploxeralf	520	15.0	78	rain
Inks	Blue oak	BO-1	*Q. douglasii, Q. wislizenii*	loamy-skeletal, mixed, superactive thermic Lithic Ultic Haploxeroll	160	17.0	46	rain

† Named for the dominant vegetative community or overstory species.

‡ Based on Soil Survey Staff (2003), using data collected from this study. Taxonomic classification may differ from the official soil series description for the mapped soil series.

§ MAT, mean annual temperature; MAP, mean annual precipitation; MAT and MAP taken from the PRISM data set (Daly et al., 1994); Precip., dominant form of precipitation.

¶ Not official soil series names; areas are currently not mapped so arbitrary names were applied.

a numerical value indicating their relative position (elevation) along the transect: blue oak (BO-1); pine–oak (PO-2); ponderosa pine (PP-3); white fir (WF-4); red fir (RF-5); subalpine (SA-6); and alpine (AL-7).

The parent material at each site consists of Miocene- to Pliocene-aged andesitic lahar, deposited as part of the Mehrten formation (Piper et al., 1939). Although the andesitic lahar material is assumed to be similar in composition across the gradient, we acknowledge that some differences in parent material may arise from possible late-Pleistocene to early-Holocene volcanic ash input or eolian deposition of silts and soluble salts from the dry east side of the Sierra Nevada. We assume, however, that differences in soil genesis resulting from variation in parent materials are small relative to the effects of climate. The presence of rounded cobbles within the low-elevation (BO-1 and PO-2) pedons suggests the parent material of these sites may be reworked lahar material derived from higher elevations. There was no evidence of glaciers reworking high-elevation materials, although the high-elevation sites probably had a permanent snowpack during glacial episodes. The geomorphic age is difficult to constrain, but is assumed to be similar among sites, with the assumption that soil properties are in a relative steady state with mid- to late-Holocene climate conditions. Three pedons, separated horizontally by roughly 15 m, were sampled at each field site. All sampling sites were on summit positions, with a west to southwest aspect and slopes averaging 10 to 15%. Sampled pedons did not exhibit evidence of human perturbation or accelerated erosion.

Soil Characterization

Soil morphology was described in the field and samples collected by morphologic horizon (Soil Survey Staff, 1999). All analyses were performed on the air-dried, <2-mm fraction (fine-earth fraction) unless otherwise noted. Bulk density of surface soils (three replicates per horizon) was measured in the field using a hammer corer device (Blake and Hartge, 1986) for one pedon in each biome. Sample weight and volume were corrected for coarse fragment content (Soil Survey Staff, 1996). For subsurface horizons, the high coarse fragment content made coring infeasible; therefore, we used bulk density data from field samples available from the NRCS Soil Survey Laboratory database (http://ssldata.nrcs.usda.gov/, verified 12 Sept. 2006) for the respective soil series located near our sampling sites.

Particle-size analysis was determined by the pipette method and wet sieving (Soil Survey Staff, 1996). Samples were pretreated with NaOCl at pH 9.5 to remove organic matter, and citrate–dithionite to remove "free" Fe oxides, and subsequently dispersed with dilute sodium hexametaphosphate. Dispersed samples were wet sieved at 53 μm, and clay and silt (material <53 μm) collected for pipette analysis. Sands (>53 μm) were collected, dried at 105°C, and weighed. Soil pH was measured 1:1 in H_2O, 1:2 in 0.01 *M* $CaCl_2$, and 1:1 in 1.0 *M* KCl (Soil Survey Staff, 1996). Organic C and N were measured by dry combustion using a Carlo-Erba C/N analyzer (Carlo-Erba Strumentazione, Rodano, Italy). Phosphate retention was determined using the method of Blakemore et al. (1981). Cation exchange capacity (CEC) was measured by BaOAc saturation and Ca replacement (Janitzky, 1986), whereas extractable cations were measured with 1 *M* NH_4OAc (pH 7.0) extraction (Soil Survey Staff, 1996). Base saturation was calculated as the sum of bases by 1 *M* NH_4OAc divided by the BaOAc CEC. All mass percentage calculations are reported on an oven-dry basis.

Mineralogical Analysis

X-ray diffraction (XRD) was performed on the clay (<2 μm), silt (2–53 μm), and very fine sand (53–100 μm) fractions for each horizon of the central pedon in each biome. Clays and silts were collected by repeated mixing and centrifugation with dilute Na_2CO_3. X-ray analyses were made with a Diano XRD 8000 diffractometer (Diano, Woburn, MA) producing Cu-Kα radiation generated with 40-kV accelerating potential and 20-mA tube current. Clays and silts were oriented on glass slides with the following standard treatments: Mg saturation, Mg saturation and glycerol solvation, K saturation, and heat treatment of K-saturated samples at 350 and 550°C (Whittig and Allardice, 1986). Halloysite was distinguished from kaolinite by the presence of a peak near 1.0 nm after intercalation with formamide (Churchman, 1990). Very fine sands were analyzed using random powder mounts.

Selective dissolution was performed on the fine-earth fraction by nonsequential extractions using sodium pyrophosphate, acid ammonium oxalate, and citrate–dithionite (Soil Survey Staff, 1996). Samples were shaken for 15 h with 0.1 *M* sodium pyrophosphate at pH 10 and a soil/liquid ratio of 1:100 to extract Al (Al_p) bound in organo–metal complexes. Samples were shaken for 4 h in the dark with a soil/oxalate ratio of 1:100 with 0.2 *M* ammonium oxalate adjusted to pH 3.0 with oxalic acid to extract Al, Fe, and Si (Al_o, Fe_o, and Si_o) from organic complexes and SRO Fe oxyhydroxides (e.g., ferrihydrite) and aluminosilicates (e.g., allophane and imogolite). Citrate–dithionite extraction consisted of shaking 4 g of soil for 15 h with 2 g of sodium dithionite and 100 mL of 0.3 *M* sodium citrate to extract Fe and Al (Fe_d and Al_d) from organic complexes, some SRO aluminosilicates, and secondary forms of Fe oxyhydroxides (Parfitt and Childs, 1988; Dahlgren, 1994). Aluminum and Fe concentrations were determined by atomic absorption spectrophotometry, and Si was determined colorimetrically (Weaver et al., 1968).

Volcanic glass counts were performed using the very fine sand fraction of selected surface and subsurface horizons. Very fine sands were mounted on glass slides with a refractive index oil of 1.54 and observed under polarized light with a gypsum first order red accessory (Cady et al., 1986). A minimum of 500 grains per sample were counted using an Olympus BH2 optical microscope.

Total elemental analysis of the fine-earth fraction from selected surface and subsurface horizons from each sample site was performed by lithium borate fusion with inductively coupled plasma–atomic emission spectrometry quantification at ACME Analytical Laboratories, Ltd. (Vancouver, BC). Selected surface and subsurface soil material from the three pedons at each site were composited separately for elemental analysis. Reported oxide values represent the average of composite surface and subsurface horizons at each site.

Clay fractions separated during the particle-size analysis were collected from the same surface and subsurface horizons as for bulk soil elemental analysis. The clay fractions (which were pretreated to remove organic matter and free Fe oxides and Na saturated during the particle-size analysis) were dialyzed to remove excess salts and total elemental analysis determined using an electron microprobe (Cameca SX-100, Cameca Instruments, Trumbull, CT). Ground, air-dry, dialyzed clays were fused on a strip heater using a low voltage, high amperage source and quenched to form a glass bead in a container pressurized with Ar gas (Brown, 1977). Glass beads were mounted and polished as thin sections, and coated with C before microprobe analysis (Sawhney, 1986). Samples were analyzed for Al, Fe, Si, Ti, Mg, Ca, Na, and K. Clay structural formulas for sites SA-6 and Al-7 (both dominated by 2:1 layer silicates) were calculated from the elemental data following Moore and Reynolds (1998), assuming a monomineralic clay fraction of 2:1 minerals and 22 charge equivalents per unit cell.

RESULTS AND DISCUSSION

Pedon Characterization

pH and Base Saturation

Soil pH values in H_2O ranged between 5.7 and 6.4 and showed no distinct trend with increasing elevation (Table 2). This is in sharp contrast to similar elevation gradients on granite and basalt parent materials in the Sierra Nevada and Cascade ranges, where pH steadily declined with increasing elevation (Alexander et al., 1993; Dahlgren et al., 1997a). Soil pH in KCl averaged 5.1 across all sites, with only the surface and subsurface horizons of SA-6 (pH in KCl of 4.3 and 4.2, respectively) indicating minor amounts of exchangeable Al^{3+} (Soil Survey Staff, 1996). Delta pH values [$\Delta pH = pH(KCl) - pH(H_2O)$] ranged between −0.7 and −1.8, indicating that all the sites were dominated by a net negative surface charge (Soil Survey Staff, 1996). In general, subsurface base saturation decreased with increasing elevation, except for the upper two sites, which showed a large relative increase (i.e., AL-7 subsurface base saturation of 60% relative to subsurface RF-5 of 10%). The unexpectedly high pH and base saturation in the upper elevation sites may result from decreased leaching, due in part to the majority of the snow-dominated precipitation being lost to runoff during spring melt and not infiltrating the soil profile. Alternatively eolian deposition of base-cation-rich playa deposits and evaporites sourced from the dry east side of the Sierra Nevada, such as the Carson basin (Johnson et al., 1997; Reheis, 1999; Cohn et al., 2004), may have contributed to elevated base saturation. Sand/silt ratios of the upper elevation sites (Table 2) do not indicate a large flux of silt-sized eolian material to the soil surface, suggesting the former mechanism may provide the best explanation. The input of soluble salts from the dry east side cannot be discounted, however.

Base saturation patterns within a given pedon indicated substantial variation between biomes dominated by conifer species (PP-3, WF-4, RF-5, and SA-6) and those dominated by grasses and oaks (BO-1, PO-2, and AL-7) (Table 2). In particular, BO-1, PO-2, and AL-7 displayed a depletion of base cations in surface horizons relative to subsurface horizons, whereas PP-3, WF-4, and RF-5 displayed enrichment in surface horizons and substantial base cation depletion in subsurface horizons. This pattern may reflect differences in the intensity of cation leaching or differential nutrient cycling dynamics among vegetation types (e.g., conifer species redistributing cations from subsurface to surface horizons via root uptake and litter deposition; Buol et al., 2003).

Organic Carbon

Maximum surface soil organic C content (on a mass percentage basis) increased with increasing elevation to a peak in WF-4 (increasing from 36 to 120 g kg^{-1} in BO-1 to WF-4), and subsequently declined at higher elevations (from 82 to 42 g kg^{-1} in RF-5 to AL-7) (Table 2). Soil C content variation across the gradient, particularly in WF-4, is probably due to the presence of SRO materials that provide numerous adsorption sites for C coupled with Al–humus complexation that inhibits biodegradation of organic C (Saggar et al., 1996; Yuan et al., 2000; Parfitt et al., 2002; Rasmussen et al., 2006). Indeed, regression of total pedon Al–humus complexes (Al_p, kg m^{-2}) vs. total pedon soil C (kg m^{-2}), indicated a highly significant correlation between these two variables ($r^2 = 0.95$; $P < 0.0001$).

Table 2. Characterization data for soils derived from andesite along an elevation and climate gradient in the Sierra Nevada of California.

Biome	Horizon	Depth	Munsell color		D_b†	Sand	Clay	Sand/silt	C	C/N	CEC‡	BS§	pH (H_2O)¶	pH ($CaCl_2$)¶	pH (KCl)¶
			Dry	Moist											
		cm			g cm^{-3}	— g kg^{-1} —			g kg^{-1}		cmol$_c$ kg^{-1}	%			
Alpine (AL-7)	A1	0–17	10YR 4/3	10YR 2/2	0.7	577	116	1.9	42	13	29	45	5.9	5.0	4.5
	A2	17–34	10YR 5/3	10YR 2/3	0.9	613	122	2.3	22	11	21	47	6.1	5.1	4.6
	AC	34–49	10YR 5/3	10YR 3/3	1.1	622	118	2.4	8	8	16	60	6.2	5.1	4.4
	Cr	fractured andesitic breccia													
Subalpine (SA-6)	A1	0–7	10YR 4/2	10YR 2/2	0.6	691	105	3.4	62	24	30	45	5.8	4.9	4.3
	A2	7–19	10YR 5/3	10YR 3/2	0.7	655	123	2.9	21	22	20	46	5.8	4.8	4.2
	AC1	19–37	10YR 5/3	10YR 2/3	0.8	694	127	3.9	12	17	19	53	6.0	4.8	4.2
	AC2	37–62	10YR 5/3	10YR 2/3	0.9	582	141	2.1	10	17	21	54	6.0	4.9	4.2
	Cr	fractured andesitic breccia													
Red fir (RF-5)	A1	0–8	10YR 4/2	10YR 2/2	0.5	645	54	2.1	82	23	17	32	6.0	5.3	4.9
	A2	8–24	10YR 4/3	10YR 2/3	0.7	601	72	1.8	43	22	12	19	6.0	5.3	5.1
	Bw1	24–38	10YR 4/3	10YR 2/3	0.7	605	53	1.8	33	20	12	10	5.8	5.2	5.1
	Bw2	38–57	10YR 4/3	10YR 2/3	0.8	625	51	1.9	23	18	12	10	5.7	5.1	5.0
	BC	57–79	10YR 5/3	10YR 3/3	0.8	628	90	2.2	24	21	13	11	5.7	4.9	4.8
	Cr	fractured andesitic breccia													
White fir (WF-4)	A1	0–19	7.5YR 4/3	7.5YR 2/2	0.5	619	41	1.8	120	23	40	51	6.3	5.5	5.1
	A2	19–32	7.5YR 5/4	7.5YR 2/3	0.7	584	62	1.7	69	23	27	25	6.2	5.3	5.1
	Bw1	32–48	7.5YR 5/4	7.5YR 3/3	0.8	656	62	2.3	46	21	23	14	6.0	5.1	5.0
	Bw2	48–83	7.5YR 5/4	7.5YR 3/3	0.9	694	63	2.9	31	20	18	11	5.9	5.0	4.9
	Cr	fractured andesitic breccia													
Ponderosa pine (PP-3)	A	0–10	7.5YR 3/4	7.5YR 2/3	0.9	382	243	1.0	89	23	44	44	6.2	5.5	5.1
	ABt	10–40	5YR 4/4	5YR 2/4	1.0	337	308	0.9	27	22	22	31	6.4	5.4	5.1
	Bt1	40–60	5YR 4/6	2.5YR 3/4	1.2	423	354	1.9	17	23	20	28	6.3	5.2	4.9
	Bt2	60–100	5YR 4/6	2.5YR 3/6	1.2	346	402	1.4	5	16	17	34	6.1	4.9	4.7
	Bt3	100–158	5YR 5/6	2.5YR 3/6	1.3	326	429	1.3	3	14	16	34	5.9	4.7	4.5
	Bt4	158–200	5YR 5/6	2.5YR 3/6	1.4	346	426	1.5	2	10	15	32	5.8	4.6	4.4
Pine–oak (PO-2)	A	0–12	7.5YR 3/3	7.5YR 3/3	0.9	360	270	1.0	31	13	27	45	5.9	5.1	4.7
	ABt	12–29	5YR 4/4	5YR 2/4	1.0	301	303	0.8	16	12	23	48	6.1	5.1	4.7
	Bt1	29–45	5YR 5/6	5YR 3/3	1.1	272	392	0.8	9	10	21	54	6.2	5.2	4.8
	Bt2	45–65	5YR 5/6	2.5YR 3/4	1.2	341	387	1.2	6	10	20	51	6.3	5.3	4.9
	Bt3	65–90	5YR 5/6	2.5YR 3/4	1.2	306	310	0.8	5	13	20	50	6.2	5.4	4.8
Blue oak (BO-1)	A1	0–5	10YR 5/4	10YR 3/3	0.9	427	167	1.1	36	13	30	52	6.2	5.5	5.1
	A2	5–14	7.5YR 5/4	7.5YR 3/3	1.1	425	178	1.1	20	12	24	50	6.2	5.1	4.7
	Bw1	14–25	7.5YR 5/4	7.5YR 3/3	1.1	474	193	1.4	12	11	22	49	6.2	4.9	4.5
	Bw2	25–42	7.5YR 5/4	7.5YR 3/3	1.2	468	192	1.4	7	9	22	58	6.4	5.2	4.6
	R	consolidated andesitic breccia													

† Bulk density.

‡ Cation exchange capacity.

§ Base saturation.

¶ pH 1:1 in H20; pH 1:2 in 0.01 *M* $CaCl_2$; pH 1:1 in 1.0 *M* KCl.

Total pedon soil C content (kg m^{-2}, calculated for each horizon and summed across the entire pedon) was greatest for PP-3 (~25 kg C m^{-2}; Fig. 1). This contrasts with data from Alexander et al. (1993) and Dahlgren et al. (1997a), who found the greatest soil C stocks in RF-5 and WF-4 biomes on basalt (25 kg C m^{-2}) and granite (15 kg C m^{-2}) parent materials, respectively. The PP-3 biome corresponds with the zone of greatest net primary production, soil weathering, and solum thickness. Therefore, the high soil C content may be attributed to greater net primary production and enhanced physicochemical protection of C in the fine soil matrix (Rasmussen et al., 2005).

Mineralogy

Volcanic Glass

Volcanic glass content varied substantially across the gradient and may be a function of differential weathering envi-

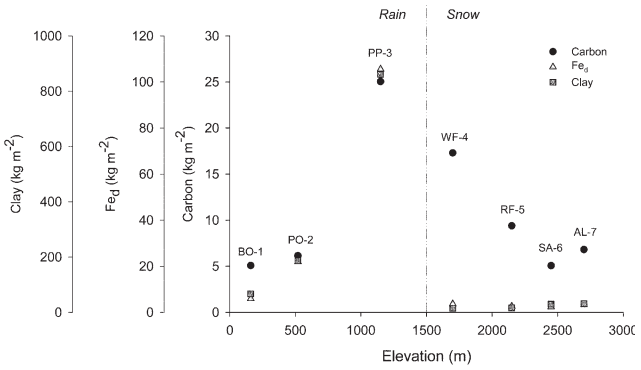

Fig. 1. Total pedon organic C, clay, and free Fe-oxide content (Fe_d) for soils derived from andesite across an elevation and climate gradient in the Sierra Nevada of California.

ronments or parent material variation, or both. Low elevation biomes (BO-1, PO-2, and PP-3) contained very little volcanic glass (<5%) in the very fine sand fractions of surface and subsurface horizons (Fig. 2). The absence suggests that glass has either been lost to weathering, as it shows the least resistance to chemical weathering (Shoji et al., 1993), or was not present in the parent material. Glass content increased significantly in WF-4 and RF-5, where precipitation changes from rain to snow dominated, suggesting a possible weathering threshold related to the form of precipitation (Fig. 2). Soils in the SA-6 and AL-7 zones showed a decrease in glass content relative to WF-4 and RF-5. The reason for this decrease is unclear, but may result from enhanced weathering due to the availability of moisture from summer thunderstorms when the soils are relatively warm or possible dilution by eolian inputs as suggested by base saturation data (see above). It is also possible that some volcanic glass in the higher elevation soils originated from late-Pleistocene- and Holocene-aged volcanic eruptions

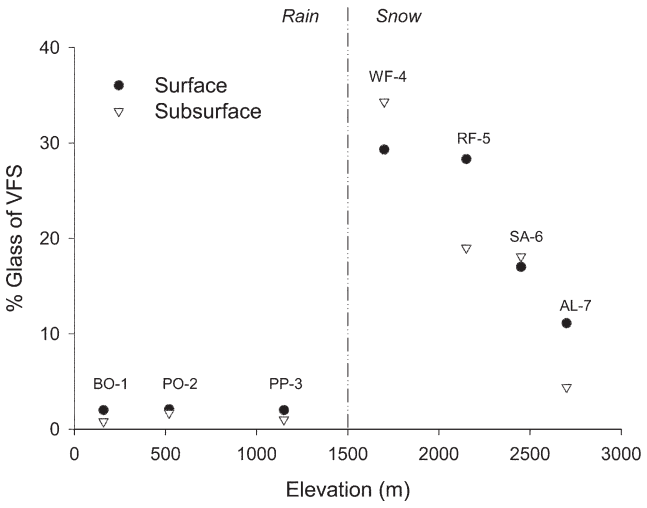

Fig. 2. Volcanic glass in the very fine sand (VFS) fraction of surface and subsurface horizons of soils derived from andesite across an elevation and climate gradient in the Sierra Nevada of California. Values for each elevation (biome) represent the following horizons: 2700 m (AL-7) A1 and AC; 2450 m (SA-6) A1 and AC2; 2150 m (RF-5) A1 and Bw2; 1700 m (WF-4) A1 and Bw1; 1150 m (PP-3) A and Bt1; 520 m (PO-2) A and Bt1; and 160 m (BO-1) A1 and Bw2.

in the Mono and Inyo basins located approximately 400 km southeast of the study sites (Wood, 1977), which would complicate our assumption of homogeneous soil age and parent material across the entire transect. For example, Burkins et al. (1999) found pumiceous glass shards disseminated throughout soils derived from granitic till in subalpine soils at elevations between 1940 and 2175 m in Yosemite National Park, roughly 320 km south of our study sites.

X-Ray Diffraction Analysis

Very Fine Sand Fraction. The XRD data for the very fine sand fraction indicated a similar primary mineral assemblage between sites with varying degrees of weathering that may be related to climate and form of precipitation (Fig. 3). General patterns between biomes suggested a preponderance of primary minerals—amphibole, plagioclase, cristobalite, and quartz. Optical analysis of the very fine sand fraction in AL-7 and SA-6 confirmed the presence of hornblende, andesine, and albite, with some apparent hydrothermal alteration and zoning of the feldspars. The XRD data for a rock sample (collected from the AL-7 site) indicated a similar mineral assemblage to that of the very fine sand fractions, but also contained tridymite as indicated by peaks at 0.411 (on the shoulder of the cristobalite peak at 0.405 nm) and 0.433 nm, and a chlorite-like material with a broad peak near 1.5 nm. The similarity in primary mineral assemblage between biomes and the andesite rock sample indicated that the parent rock composition was similar between sites.

A 0.7-nm kaolin peak was present in all biomes except for AL-7. The 0.7-nm peak became progressively more prominent at lower elevations, with an abrupt increase in its dominance noted in the rain-dominated, low-elevation sites (Fig. 3). The increased dominance of the 0.7-nm peak was coupled with a loss of many of the plagioclase peaks apparent in the snow-dominated sites, suggesting a direct in situ transformation of feldspar to halloysite (e.g., Hendricks and Whittig, 1968a; Southard and Southard, 1987). The 0.334-nm quartz peak demonstrated a significant increase in intensity in the rain-dominated sites, indicating a mass loss of other primary minerals and concentration of quartz in the sand fraction. The PP-3 patterns also showed a gibbsite peak (0.484 nm), further indicating the extreme weathering and desilication environment in this biome. It should also be noted that the abundance of feldspar increased in the BO-1 biome relative to the other rain-dominated sites, suggesting that the relatively low rainfall at this site (Table 1) limits primary mineral weathering.

Silt Fraction. X-ray diffraction of the silt fractions indicated a similar mineral assemblage across all biomes—a mixture of plagioclase feldspars, hornblende, cristobalite, and quartz, as well as kaolin minerals and an interlayered 2:1 mineral (Fig. 4). The similarity in mineral assemblage across all sites again strongly suggested relative uniformity of parent rock across the gradient. The overall patterns were very similar to those discussed for the very fine sand fraction. The kaolin peak (0.7 nm) was only very weakly expressed in AL-7 and increased in intensity and peak sharpness from SA-6 to BO-1. Similarly, there was an increase in a 1.0-nm peak from RF-5 to BO-1 that may be

attributed to either a vermiculite-like 2:1 mineral or 1.0-nm halloysite. There was a distinct transition in silt mineral assemblage from snow-dominated to rain-dominated sites in that PP-3 and PO-4 demonstrated (i) loss of plagioclase feldspar peaks and a increase in kaolin peaks (0.7 nm), (ii) an increase in the intensity of the 0.334-nm quartz peak, and (iii) PP-3 showed a gibbsite peak (0.484 nm). All these parameters indicated a significant increase in primary mineral weathering and secondary mineral neogenesis relative to snow-dominated biomes. The BO-1 biome demonstrated a sharp 0.7-nm peak and a reemergence of prominent primary mineral peaks.

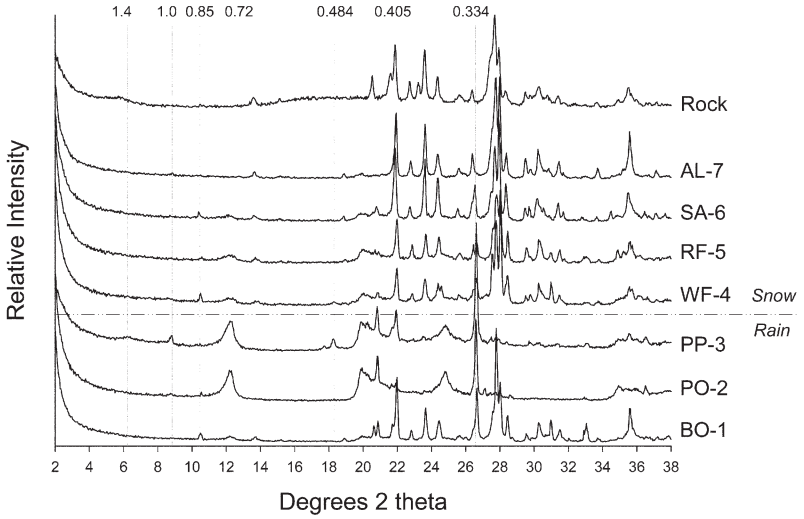

Fig. 3. X-ray diffractograms for random powder mounts of Mg^{2+}-saturated 25°C very fine sand fractions from subsurface horizons of each biome along an elevation and climate gradient on andesite parent materials in the Sierra Nevada, California. The horizons shown from each respective biome are: AL-7, A2; SA-6, A2; RF-5, Bw1; WF-4, Bw1; PP-3, Bt1; PO-2, Bt1; and BO-1, Bw1. The break between PP-3 and WF-4 represents the transition from rain-dominated systems to snow-dominated systems. Drop lines are in nanometers; unlabeled peaks dominantly derive from feldspars.

Clay Fraction

X-ray diffraction of the clay fractions indicated that AL-7 and SA-6 were dominated by crystalline minerals—partially interlayered 2:1 minerals with smaller amounts of poorly ordered kaolin minerals (broad 0.7-nm peak that disappears with 550°C treatment; Fig. 5). The K^+-saturated 1.4-nm peak exhibited only partial collapse with heating to 550°C, and exhibited moderate swelling with Mg^{2+} saturation and glycerol solvation, suggesting a partially interlayered smectite-like mineral. The XRD analysis of the clay fraction isolated from ground andesite lithic material (Mg^{2+} saturated and oriented on a glass slide) from these sites indicates the presence of a chlorite-like mineral, with a broad peak from 1.4 to 2.9 nm that does not swell with Mg^{2+} saturation and glycerol solvation. The chlorite-like mineral suggests that the 2:1 mineral phases in the clay fraction were inherited from the parent material rather than through neogenesis. This is in agreement with previous studies indicating the presence of chlorite, mixed chlorite–smectite, and smectite minerals in volcanic ash deposits (Glasmann, 1982; Pevear et al., 1982; Dahlgren and Ugolini, 1989). These mixed layer minerals may form through hydrothermal alteration and pseudomorphic transformation of primary minerals (e.g., pyroxene or plagioclase) during and before eruption, with the degree of "chloritization" dependent on temperature. Smectite and swelling chlorite are reported to form between 200 and 230°C, and fully interlayered chlorite above 230°C in hydrothermal environments (Fan, 1979; Kristmannsdottir, 1979). As noted above, eolian deposition may be an active process in these biomes (as suggested by the unexpectedly high base saturation) and cannot be ruled out as an additional source of 2:1 minerals; however, eolian deposition would be expected to preferentially enhance the 2:1 mineral abundance in the surface horizons, which was not the case for SA-6 and AL-7.

The WF-4 and RF-5 clay fractions were dominated by x-ray amorphous materials, although XRD patterns indicate traces of 2:1 and 0.7-nm kaolin minerals (Fig. 6). The RF-5 2:1 mineral displayed slight expansion with Mg saturation and glycerol solvation and incomplete collapse with K saturation and heating, suggesting an expansible smectite-like species, similar to that observed in SA-6 and AL-7 but with a greater degree of interlayering. In contrast to RF-5, SA-6, and AL-7, the WF-4 2:1 mineral did not expand with Mg saturation and glycerol solvation and demonstrated only partial collapse of K-saturated samples with heating, indicating a fully interlayered mineral. The 0.7-nm peak in both WF-4 and RF-5 tends to broaden with soil depth, and formamide treatment of subsurface horizons induced a shift in the 0.7-nm peak toward 1.0 nm, suggesting halloysite in the subsurface clay fractions (data not shown).

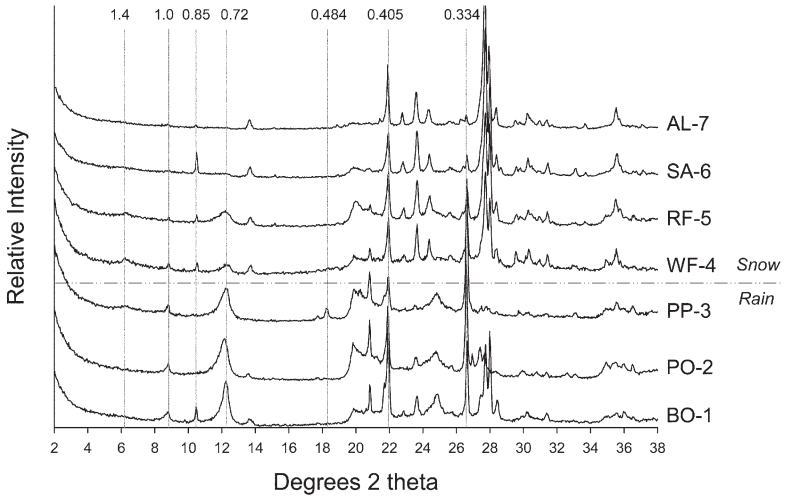

Fig. 4. X-ray diffractograms for oriented Mg^{2+}-saturated 25°C silt fractions from subsurface horizons of each biome along an elevation and climate gradient on andesite parent materials in the Sierra Nevada, California. The horizons shown from each respective biome are: AL-7, A2; SA-6, A2; RF-5, Bw1; WF-4, Bw1; PP-3, Bt1; PO-2, Bt1; and BO-1, Bw1. The break between PP-3 and WF-4 represents the transition from rain-dominated systems to snow-dominated systems. Drop lines are in nanometers; unlabeled peaks dominantly derive from feldspars.

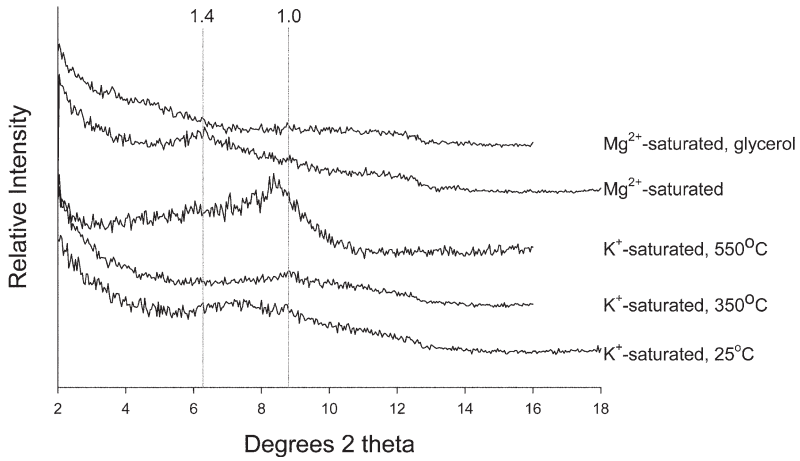

Fig. 5. X-ray diffractograms for the clay fraction of the Alpine (AL-7) biome surface horizon. Drop lines are in nanometers.

The BO-1, PO-2, and PP-3 clay fractions were dominated by kaolin minerals, as evidenced by a distinct 0.7-nm peak (Fig. 6). The kaolin mineral was predominantly kaolinite or dehydrated 0.7-nm halloysite in the PP-3 surface horizons, with greater dominance of halloysite with increasing depth, as indicated by a nearly complete shift of the 0.7-nm peak to 1.0 nm with Mg^{2+} saturation and formamide solvation in subsurface horizons (Fig. 7). The shift to halloysite with depth may be explained by dehydration of halloysite in surface soils due to extreme summer drying in the xeric soil moisture regime of California (Southard and Southard, 1987, 1989; Takahashi et al., 1993, 2001). Takahashi et al. (2001) provided evidence that halloysite dehydration was the main mechanism for the difference in kaolin mineralogy between surface and subsurface horizons of an andesitic Haploxeralf near Mt. Shasta, California—the morphology of observed tubular halloysite did not change with depth, whereas expansion with formamide solvation showed a progressive transition. The subsurface horizon clay fractions of PO-2 also displayed minor swelling with Mg^{2+} saturation and formamide solvation, although the peak shift was poorly expressed (data not shown), suggesting greater halloysite dehydration relative to PP-3 throughout the profile. This pattern fits with the climate pattern of less precipitation and higher soil temperature in PO-2, relative to PP-3, producing a more pronounced drying of the soil profile.

The PO-2 and PP-3 clay fraction diffractograms also indicated the presence of a fully interlayered 2:1 mineral, as evidenced by incomplete collapse of K^+-saturated samples with heating. The persistence of the 2:1 mineral in this intense weathering regime may be attributed to stabilization by Al interlayering (Barnhisel and Bertsch, 1989; Nieuwenhuyse and van Breemen, 1997; Ndayiragije and Delvaux, 2003). In addition, PP-3 diffraction patterns indicated the presence of gibbsite throughout the profile. The gibbsite peak increased in size and intensity with depth, suggesting either greater gibbsite content or a more crystalline species (data not shown). Precipitation and crystallinity of gibbsite in the surface horizon may be inhibited by organic interactions with Al, as indicated by greater concentrations of SRO Al and Al–humus complexes in surface horizons (see below and Table 3). Gibbsite in the subsurface horizons was probably derived from desilication of kaolin or pseudomorphic transformation of feldspar (Mulyanto et al., 1999; Rasmussen et al., 2005), as suggested by the presence of gibbsite in the silt and very fine sand fractions.

The clay fraction in BO-1 was dominated by 2:1 and 1:1 minerals (Fig. 6). The K^+-saturated 2:1 mineral displayed partial collapse in surface horizons and greater collapse with heating to 550°C at depth, suggesting less interlayering in subsurface horizons (data not shown). In contrast to the high-elevation biomes, the 2:1 mineral did not expand with Mg^{2+} saturation and glycerol solvation, suggesting a nonexpansible vermiculite-like 2:1 mineral rather than the expansible smectite-like mineral noted in high-elevation biomes. The 0.7-nm peak broadened with Mg^{2+} saturation and formamide solvation, but did not shift toward a 1.0-nm peak. The hot, dry environment experienced by this soil probably promotes dehydration of halloysite.

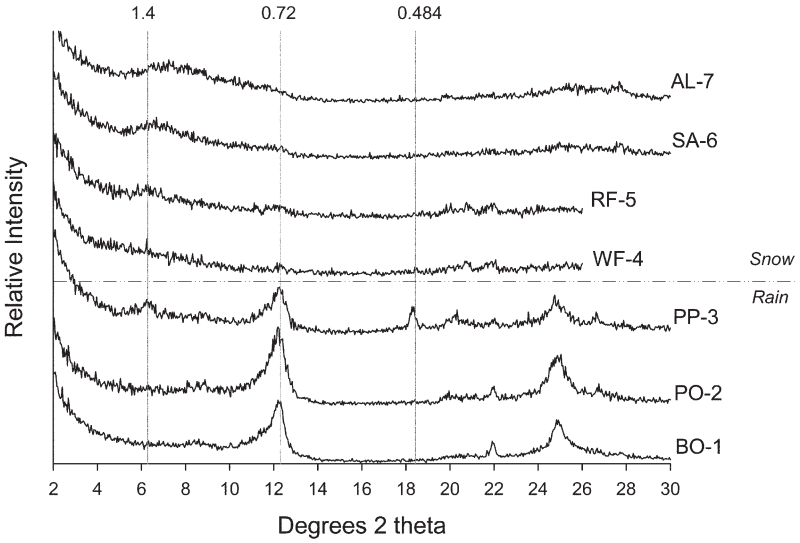

Fig. 6. X-ray diffractograms for K^+-saturated 25°C clay fractions from subsurface horizons of each biome along an elevation and climate gradient on andesite parent materials in the Sierra Nevada, California. The horizons shown from each respective biome are: AL-7, A2; SA-6, A2; RF-5, Bw1; WF-4, Bw1; PP-3, Bt1; PO-2, Bt1; and BO-1, Bw1. The break between PP-3 and WF-4 represents the transition from rain-dominated systems to snow-dominated systems. Drop lines are in nanometers.

Selective Dissolution

Iron Oxides and Oxyhydroxides

Iron oxide and oxyhydroxide content varied considerably between biomes (Table 3). Crystalline Fe oxide content was greatest in PP-3, as indicated by a substantial Fe_d content (37–53 g kg^{-1}) on a mass basis, and minimal Fe_o relative to Fe_d (Fe_o/Fe_d < 11% in all horizons). The dominance of crystalline Fe oxides in PP-3 indicated a highly weathered soil, where a large portion of Fe has been released from primary minerals and precipitated as free Fe oxides. A comparison of Fe_d to total Fe (Fe_t) of the

fine-earth fraction indicated that >80% of Fe_t occurred as Fe_d (Table 4). This indicator of strong weathering is in agreement with XRD data, indicating secondary weathering products in the silt and very fine sand fractions. The PO-2 biome also contained a significant portion of its free Fe oxides in crystalline form (Fe_o/Fe_d < 12%) and an average Fe_d/Fe_t of 65% throughout the pedon. The Fe_o/Fe_d increase for BO-1 relative to PO-2 and PP-3 suggests somewhat less crystalline Fe oxides, possibly due to higher Si concentrations associated with lower leaching that impedes Fe oxide crystallization (Schwertmann, 1985). The Fe_d/Fe_t percentage in BO-1 was <35% and suggests a decreased weathering intensity, probably due to drier conditions relative to PO-2 and PP-3.

In contrast to low-elevation biomes, mid- and high-elevation biomes (WF-4, RF-5, SA-6, and AL-7) all contained a significant portion of noncrystalline Fe oxyhydroxides (Fe_o/Fe_d of 40–50%; Table 4). The higher organic matter concentrations and colder soil temperatures may inhibit crystallization in the snow-dominated biomes (Schwertmann, 1985; Schwertmann and Taylor, 1989). The Fe_d/Fe_t was <30% in these biomes, indicating a less intense weathering environment than the rain-dominated biomes. The low weathering intensity indicated by Fe_d/Fe_t was in agreement with volcanic glass contents and XRD data, indicating that primary minerals dominate the silt and very fine sand fractions of the higher elevation biomes.

Short-Range Ordered Aluminosilicates and Aluminum–Humus Complexes

Short-range ordered aluminosilicates were only present to a significant extent in WF-4 and RF-5, as indicated by Al_o and Si_o concentrations and a $(Al_o - Al_p)/Si_o$ ratio near 2.0 (Table 3). Estimates of the percentage of allophane by weight for WF-4 and RF-5 nearly equaled the percentage of clay by weight determined by particle-size analysis, suggesting that the majority of the clay fraction in these biomes may be composed of SRO materials. This agrees with XRD data indicating few crystalline minerals in the clay fraction. The presence of allophane spheres and imogolite tubes in the clay fraction of these biomes was verified by transmission electron microscopy.

We originally hypothesized that the dominance of SRO aluminosilicate materials would increase with increasing elevation. Cooler soil temperatures and less severe desiccation of the profile in the snow-dominated zone were expected to hinder crystallization, thereby contributing to preferential formation of allophane and imogolite. Allophane and imogolite were not detectable in the cryic soil temperature regime, however. It is possible that cold soil temperatures limit the release of Al and Si from primary minerals. Nevertheless, using Fe_d (Table 3) or Fe_d/Fe_t (Table 4) values as a measure of weathering, there is little difference in overall weathering intensity between the frigid and cryic zones. Alternatively, SRO aluminosilicate formation may be limited by competition for dissolved Al by complexation with organic matter or interlayering of 2:1 layer silicates, the antiallophanic effect (Shoji et al., 1993; Dahlgren et al., 1997b). Aluminum–humus complexes comprised >50% of the extractable Al species (Al_p/Al_o), which may inhibit allophane and imogolite precipitation (Shoji et al., 1993). In contrast, chemical weathering in the mesic and frigid biomes (WF-4 and RF-5) may be sufficient to release enough Al so that organic matter and the interlayers of 2:1 layer silicates are appreciably saturated and no longer able to act as sinks for dissolved Al. The absence of SRO aluminosilicates in low-elevation biomes (BO-1, PO-2, and PP-3) implies (i) that high solution silica activities promoted formation of kaolins rather than SRO materials during mineral neogenesis (Parfitt et al., 1983), (ii) that any preexisting SRO aluminosilicates have been transformed to crystalline minerals or lost due to weathering and dissolution, or (iii) a lack of volcanic glass in the parent material.

Total Elemental Analysis

In general, weathering intensity determined from base cation (Ca^{2+}, Mg^{2+}, Na^+, and K^+) concentrations in the <2-mm fraction followed other weathering indicators (Table 4). Using Na_2O + CaO as an indicator of leaching or weathering intensity suggests the following (strong to weak): PP-3 ∼ PO-2 > WF-4 ∼ RF-5 ∼ BO-1 > SA-6 ∼ AL-7. The large increase in Na_2O + CaO in SA-6 and AL-7 may be a function of eolian input because Fe_d/Fe_t values were similar between the frigid and cryic soil temperature regimes, indicating similar weathering regimes. Dilution of the very fine sand fraction by eolian input may also partially explain the decrease in volcanic glass content determined in SA-6 and AL-7, although the sand/silt ratios (Table 2) and lack of exotic minerals in the very fine sand and silt fractions do not support significant eolian deposition. Alternatively, leaching may be lower in high-elevation biomes because of limited water infiltration into the soil profile during snowmelt.

Clay structural formulas were calculated from microprobe elemental data for SA-6 and AL-7, assuming a monomineralic clay fraction composed of 2:1 layer silicates. This assumption more than likely oversimplified the actual clay mineral assemblage, but provided some indication of possible mineral transformations. The calculated formulas suggest an interlayered, tetrahedrally substituted, dioctahedral 2:1 mineral in both biomes, assuming posi-

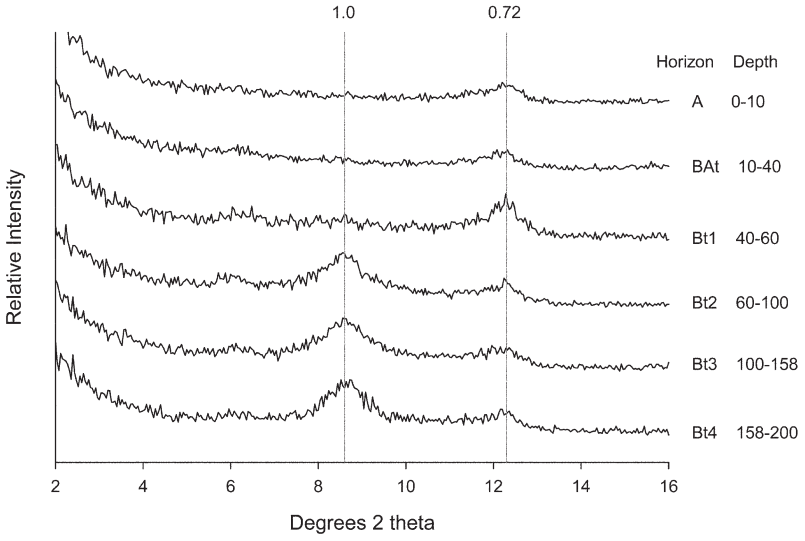

Fig. 7. X-ray diffractograms of Mg^{2+}-saturated and formamide-solvated clays from all horizons of the PP-3 biome. Drop lines are in nanometers. The 1.0-nm peak represents expansion of the halloysite 0.72-nm peak.

Table 3. Selective dissolution data for soils derived from andesite along an elevation and climate gradient in the Sierra Nevada of California.

Biome	Depth	Fe_d†	Al_d†	Fe_o‡	Al_o‡	Si_o‡	Fe_p§	Al_p§	$(Al_o - Al_p)/Si_o$	Allophane¶	P retention#	$Al_o + ½Fe_o$	Fe_o/Fe_d
	cm	g kg^{-1}							molar ratio	g kg^{-1}	%	g kg^{-1}	
Alpine (AL-7)	0–17	12.9	3.6	6.7	6.1	0.8	2.5	2.7	4.2	–	48	9.5	0.52
	17–34	12.2	3.3	6.0	6.4	1.2	2.4	2.5	3.3	–	50	9.4	0.50
	34–49	12.0	2.1	5.2	4.3	0.8	1.6	1.4	4.1	–	38	6.9	0.43
Subalpine (SA-6)	0–7	10.1	3.8	4.5	6.4	0.7	1.6	3.4	4.5	–	53	8.7	0.45
	7–19	10.4	3.5	4.9	7.4	1.1	1.4	2.9	4.2	–	58	9.9	0.48
	19–37	10.2	2.6	4.4	6.5	1.2	0.8	1.8	4.0	–	52	8.8	0.43
	37–62	9.6	2.2	4.1	6.1	1.2	0.8	1.5	3.8	–	49	8.2	0.43
Red fir (RF-5)	0–8	8.7	6.6	5.3	27.0	7.7	0.8	8.3	2.5	77	86	29.7	0.61
	8–24	11.2	6.9	5.9	34.1	11.7	0.7	6.7	2.4	117	95	37.0	0.52
	24–38	11.6	6.6	6.0	34.4	12.8	0.6	5.4	2.4	128	96	37.4	0.51
	38–57	11.4	6.5	6.0	33.3	12.5	0.6	5.1	2.3	125	95	36.3	0.52
	57–79	10.3	6.3	5.5	28.5	10.6	0.6	4.8	2.3	106	94	31.2	0.54
White fir (WF-4)	0–19	13.0	11.2	6.5	31.2	10.9	1.3	10.5	2.0	77	95	34.4	0.50
	19–32	15.3	10.8	6.9	37.0	15.2	1.3	8.8	1.9	107	97	40.4	0.45
	32–48	16.0	8.7	6.9	38.6	17.8	1.0	5.9	1.9	125	96	42.0	0.43
	48–83	14.0	6.3	6.2	34.3	17.5	0.6	4.6	1.8	123	94	37.4	0.44
Ponderosa pine (PP-3)	0–10	37.4	9.9	4.3	15.2	2.7	1.2	5.9	3.5	--	87	17.3	0.11
	10–40	44.1	9.8	4.6	16.7	4.3	1.0	4.4	2.9	--	93	19.0	0.10
	40–60	47.9	9.1	4.5	14.6	3.9	0.9	3.5	3.0	--	88	16.8	0.09
	60–100	53.3	7.1	4.5	6.3	1.1	0.9	1.5	4.4	--	73	8.5	0.08
	100–158	49.0	6.8	4.6	4.6	0.9	0.5	1.1	3.8	--	65	6.9	0.09
	158–200	47.3	5.4	4.5	3.8	0.8	0.3	0.9	3.7	--	58	6.1	0.09
Pine–oak (PO-2)	0–12	32.8	3.0	3.9	3.7	0.5	0.7	1.1	5.0	--	43	5.7	0.12
	12–29	36.8	3.1	4.0	3.7	0.6	0.6	0.9	5.1	--	42	5.7	0.11
	29–45	39.6	2.8	4.5	3.2	0.7	0.4	0.6	4.1	--	42	5.5	0.11
	45–65	41.0	2.9	4.7	3.0	0.8	0.3	0.5	3.5	--	44	5.3	0.11
	65–90	41.3	2.8	4.9	2.8	0.9	0.2	0.4	2.8	--	41	5.3	0.12
Blue Oak (BO-1)	0–5	15.8	1.3	3.9	2.0	0.4	0.5	0.6	3.3	--	22	4.0	0.25
	5–14	16.3	1.3	4.1	2.0	0.4	0.5	0.6	3.5	--	24	4.1	0.25
	14–25	16.6	1.3	3.8	1.9	0.5	0.4	0.5	3.2	--	24	3.8	0.23
	25–42	16.4	1.2	3.3	1.6	0.5	0.3	0.3	2.5	--	23	3.3	0.20

† Citrate dithionite extraction.

‡ Acid ammonium oxalate extraction.

§ Sodium pyrophosphate extraction.

¶ Allophane content estimated by mulitplying Sio content by a multiplier according the (Alo - Alp)/Sio ratio: ratio of 2.5, muliplier of 10; ratio of 2.0, multiplier of 7 (Dahlgren, 1994).

Phosphorus retention.

tive octahedral layer charge was derived from hydroxy-interlayer material (Table 5). The 2:1 mineral was probably inherited from the parent material, as suggested by XRD data of the parent rock that indicated the presence of a chlorite-like mineral and the presence of 2:1 minerals in each soil across the transect. Interlayering (as evidenced by the excess positive charge in the octahedral sheet) increased with depth in both biomes (suggesting inheritance of a chlorite species from the parent material) and was inversely related to soil organic matter concentrations. Increased interlayering with depth suggests that the surface horizons experience a more intense weathering environment that promotes loss of interlayer material from the chlorite interlayer position. Such loss is particularly evident in the surface horizons of SA-6, where hydroxy interlayering was minimal. The apparent loss of interlayer material with greater weathering discounts the "antiallophane" effect of interlayer Al sequestration in the organic-matter-rich upper horizons. Rather, inhibition of allophane and imogolite formation in these horizons was probably due to Al–humus complexation.

Soil Taxonomy and Pedogenic Trajectories

Variation in mineralogy and physical properties were further exemplified in soil taxonomic classification (Soil Survey Staff, 2003) across the environmental gradient (Table 1). Indicators of soil development (clay content, reddening, and argillic hori-

zon expression) increased with increasing elevation, reaching a maximum in the PP-3 biome, and subsequently decreased at higher elevations (Fig. 1). The degree of soil development was recognized in the taxonomic classification, with soils grading from a shallow Mollisol in BO-1, to a clay-rich Alfisol in PO-2, to a highly weathered, clay- and Fe-oxide-rich Ultisol in PP-3 (Table 1, Fig. 1). There was a dramatic shift in soil properties (e.g., loss of argillic horizon and reddening) between the PP-3 and WF-4 biomes that corresponds with the shift from rain to snow as the dominant form of precipitation. Dahlgren et al. (1997a) and Alexander et al. (1993) noted similar shifts in degree of soil development on granite and basalt at the break between the PP-3 and WF-4 biomes, suggesting a threshold in weathering processes related to the shift from rain- to snow-dominated systems.

Table 4. Average total elemental analysis for the fine earth fraction of surface and subsurface horizons for soils derived from andesite across an elevation and climate gradient in the Sierra Nevada of California†.

Biome	Na_2O	CaO	K_2O	MgO	Al_2O_3	SiO_2	Fe_2O_3	Na_2O + CaO	Fe_d/Fe_t‡
	wt %								
Alpine (AL-7)	2.8	4.8	1.5	2.5	18	50	7.8	7.7	0.32
Subalpine (SA-6)	2.7	4.8	1.3	2.8	18	49	7.8	7.5	0.25
Red fir (RF-5)	1.4	2.9	0.7	3.6	21	38	9.4	4.3	0.22
White fir (WF-4)	1.1	3.0	0.8	3.2	18	35	9.4	4.1	0.29
Ponderosa pine (PP-3)	0.1	0.6	0.3	0.3	25	33	10.6	0.6	0.81
Pine–oak (PO-2)	0.3	0.5	0.7	0.5	24	43	11.1	0.8	0.65
Blue oak (BO-1)	1.6	2.8	1.0	1.8	18	50	9.8	4.4	0.33

† Values for each biome represent an average of the following horizons: AL-7, A1 and AC; SA-6, A1 and AC2; RF-5, A1 and Bw2; WF-4, A1 and Bw1; PP-3, A and Bt1; PO-2, A and Bt1; BO-1, A1 and Bw2.

‡ Ratio of dithionite-extractable Fe to total Fe.

The WF-4 and RF-5 biomes were the only biomes that exhibited andic soil properties, namely P retention >85%, Al_o + ½Fe_o >2.0%, and a soil bulk density <0.9 g cm^{-3} (Soil Survey Staff, 2003). The PP-3 biome exhibited sufficient P retention but failed to meet the Al_o + ½Fe_o and bulk density criteria, or glass content. The BO-1, SA-6, and AL-7 biomes did not meet Al_o + ½Fe_o, P retention, glass content, or bulk density requirements for andic soil properties (Table 2). The SA-6 biome was nearly classified as an Andic Dystrocryept, but was limited by a combination of Al_o + ½Fe_o and volcanic glass content.

Taxonomic classification suggests two possible soil evolutional sequences or pedogenic trajectories: one for cold, wet systems and one for warm, dry systems. The cold, wet system may be typified by progression from Inceptisol → Andisol → Ultisol, as indicated by the sequence from AL-7/SA-6 → RF-5/WF-4 → PP-3, with the degree of soil development limited by temperature. In contrast, the warm, dry weathering sequence includes progression from Mollisol → Alfisol → Ultisol, as indicated by the BO-1 → PO-2 → PP-3 sequence, with soil development limited by precipitation. These sequences converged at the highly weathered Ultisol of the PP-3 biome, where the combination of a warmer, mesic environment with abundant precipitation produces soils with low base saturation, high free Fe oxide and clay accumulation, and expression of a well-developed argillic horizon. These sequences compare with similar weathering sequences proposed for environmental gradients on andesitic parent materials in udic, tropical environments that include a progression from Entisol → Inceptisol → Andisol → Ultisol → Oxisol (Nieuwenhuyse and van Breemen, 1997; Chorover et al., 1999; Chen et al., 2001; Zehetner et al., 2003), and an Andisol → Inceptisol → Alfisol sequence described by Takahashi et al. (1993) in a mesic, xeric environment.

SUMMARY

Soil mineralogy, physicochemical properties, and taxonomic classification suggest a strong influence of climate on soil genesis and mineral transformation in soils derived from andesitic parent materials in the xeric soil moisture regime of California. Very fine sand, silt, and clay XRD data indicate that one of the dominant weathering reactions across the gradient is the direct transformation of feldspar to kaolin minerals. Low-elevation biomes demonstrated dehydration of halloysite in surface horizons, probably due to extreme desiccation and heating in summer. Data further indicate a significant break in soil development and weathering at the current permanent winter snowline (∼1590 m). Soils in the snowfall-dominated zone exhibited minimal soil development and dominance of the clay fraction by SRO materials and interlayered 2:1 minerals, whereas soils dominated by rainfall exhibited maximum soil development and dominance of the clay fraction by kaolins. Further, the very fine sand fractions of the snow-dominated systems contain relatively unweathered primary minerals, whereas rainfall-dominated regimes exhibit substantial pseudomorphic replacement of primary minerals with kaolin and gibbsite. The weathering threshold is probably an interaction between soil moisture and temperature. Low-elevation soils remain rela-

Table 5. Clay structural formula estimation for surface and subsurface horizons of soils derived from andesite in the Sierra Nevada of California.

Biome	Horizon	Clay formula†	Charge distribution‡
Alpine (AL-7)	A1	$(Ca_{0.019}, K_{0.066}, Na_{0.194})\ (Al_{1.657}, Fe_{0.372}, Mg_{0.142}, Ti_{0.051})^{VI}\ (Si_{3.501}, Al_{0.499})^{IV}\ O_{10}(OH)_2$	Tetra = −0.499 Octa = +0.202
	AC	$(Ca_{0.025}, K_{0.067}, Na_{0.224})\ (Al_{1.692}, Fe_{0.385}, Mg_{0.116}, Ti_{0.050})^{VI}\ (Si_{3.386}, Al_{0.614})^{IV}\ O_{10}(OH)_2$	Tetra = −0.614 Octa = +0.277
Subalpine (SA-6)	A1	$(Ca_{0.051}, K_{0.122}, Na_{0.224})\ (Al_{1.672}, Fe_{0.244}, Mg_{0.151}, Ti_{0.052})^{VI}\ (Si_{3.547}, Al_{0.453})^{IV}\ O_{10}(OH)_2$	Tetra = −0.453 Octa = +0.016
	AC2	$(Ca_{0.014}, K_{0.048}, Na_{0.181})\ (Al_{1.807}, Fe_{0.311}, Mg_{0.114}, Ti_{0.043})^{VI}\ (Si_{3.303}, Al_{0.697})^{IV}\ O_{10}(OH)_2$	Tetra = −0.697 Octa = +0.444

† Calculated following Moore and Reynolds (1998) assuming a 2:1 mineral structure with 22 charge equivalents per unit cell.

‡ Excess positive octahedral charge is attributed to interlayer Al-hydroxides.

tively warm during the wet winter months, promoting in situ mineral weathering. In contrast, high-elevation soils experience cold temperatures when the soil profile is moist, followed by dry conditions during the warm summer period.

The upper elevation systems may be further subdivided by clay mineral assemblage at the transition from frigid to cryic systems. The WF-4 and RF-5 biomes are dominated by allophane and imogolite in the clay fraction, along with fully interlayered 2:1 minerals. In contrast, SA-6 and AL-7 contain minimal SRO aluminosilicate materials and are dominated by a swelling 2:1 layer silicate. It is likely that the 2:1 minerals throughout the transect are inherited from the parent material based on the presence of a chlorite-like mineral found in the andestic parent material, although eolian deposition cannot be ruled out, as suggested by unexpectedly high base saturation and total Na_2O + CaO in the <2-mm fraction at the high-elevation sites.

Soil development and weathering converge at the Ultisol in the PP-3 biome. This soil represents the most highly weathered soil, dominated by kaolin minerals, gibbsite, crystalline Fe oxides, and substantial clay and organic C content. Weathering and mineral transformations at lower elevations appear to be limited by moisture, whereas higher elevation systems are limited by temperature.

ACKNOWLEDGMENTS

We thank David J. Lowe for comments that improved previous versions of this manuscript and Solomon Henson for laboratory assistance.

REFERENCES

Alexander, E.B., J.I. Mallory, and W.L. Colwell. 1993. Soil–elevation relationships on a volcanic plateau in the southern Cascade Range, northern California, USA. Catena 20:113–128.

Bakker, L., D.J. Lowe, and A.G. Jongmans. 1996. A micromophological study of pedogenic processes in an evolutionary soil sequence formed on late Quaternary rhyolitic tephra deposits, North Island, New Zealand. Quatern. Int. 34–36:249–261.

Barnhisel, R.I., and P.M. Bertsch. 1989. Chlorites and hydroxy-interlayered vermiculite and smectite. p. 729–788. *In* J.B. Dixon and S.B. Weed (ed.) Minerals in soils environments. 2nd ed. SSSA Book Ser. 1. SSSA, Madison, WI.

Blake, G.R., and K.H. Hartge. 1986. Bulk density. p. 363–375. *In* A. Klute (ed.) Methods of soil analysis. Part 1. 2nd ed. SSSA Book Ser. 5. SSSA, Madison, WI.

Blakemore, L.C., P.L. Searle, and B.K. Daly. 1981. Soil Bureau laboratory methods: A method for chemical analysis of soils. N.Z. Soil Bureau Sci. Rep. 10A. DSIRO, Lower Hutt, New Zealand.

Brown, R.W. 1977. A sample fusion technique for whole rock analysis with the electron microprobe. Geochim. Cosmochim. Acta 41:435–438.

Buol, S.W., R.J. Southard, R.C. Graham, and P.A. McDaniel. 2003. Soil genesis and classification. 5th ed. Iowa State Univ. Press, Ames.

Burkins, D.L., J.D. Blum, K. Brown, R.C. Reynolds, and Y. Erel. 1999. Chemistry and mineralogy of a granitic, glacial soil chronosequence, Sierra Nevada Mountains, California. Chem. Geol. 162:1–14.

Cady, J.G., L.P. Wilding, and L.R. Drees. 1986. Petrographic microscope techniques. p. 185–215. *In* A. Klute (ed.) Methods of soil analysis. Part 1. 2nd ed. SSSA Book Ser. 5. SSSA, Madison, WI.

California Department of Water Resources. 1952–1962. Water conditions in California. Bull. 120. Calif. Dep. of Water Resour., Sacramento.

Chadwick, O.A., and J.C. Chorover. 2001. The chemistry of pedogenic thresholds. Geoderma 100:321–353.

Chen, Z.S., T.C. Tsou, V.B. Asio, and C.C. Tsai. 2001. Genesis of Inceptisols on a volcanic landscape in Taiwan. Soil Sci. 166:255–266.

Chorover, J., M.J. DiChiaro, and O.A. Chadwick. 1999. Structural charge and cesium retention in a chronosequence of tephritic soils. Soil Sci. Soc. Am. J. 63:169–177.

Churchman, G.J. 1990. Relevance of different intercalation tests for distinguishing halloysite from kaolinite in soils. Clays Clay Miner. 38:591–599.

Cohn, S.A., J. Lewis, and J. Hallet. 2004. The February 28, 2002 Reno dust storm: A case study. *In* Conf. on the Application of Air Pollution Meteorol. with the Air and Waste Manage. Assoc., 13th. 23–25 Aug. 2004. Available at ams.confex.com/ams/pdfpapers/79805.pdf (verified 12 Sept. 2006). Am. Meteorol. Soc., Boston, MA.

Dahlgren, R.A. 1994. Quantification of allophane and imogolite. p. 430–451. *In* J.E. Amonette and L.W. Zelazny (ed.) Quantitative methods in soil mineralogy. SSSA, Madison, WI.

Dahlgren, R.A., J.L. Boettinger, G.L. Huntington, and R.G. Amundson. 1997a. Soil development along an elevational transect in the western Sierra Nevada, California. Geoderma 78:207–236.

Dahlgren, R.A., J.P. Dragoo, and F.C. Ugolini. 1997b. Weathering of Mt. St. Helens tephra under a cyric-udic climate regime. Soil Sci. Soc. Am. J. 61:1519–1525.

Dahlgren, R.A., M. Saigusa, and F. Ugolini. 2004. The nature, properties and management of volcanic soils. Adv. Agron. 82:113–182.

Dahlgren, R.A., and F.C. Ugolini. 1989. Formation and stability of imogolite in a tephritic Spodosol, Cascade Range, Washington, USA. Geochim. Cosmochim. Acta 53:1897–1904.

Daly, C., R.P. Neilson, and D.L. Phillips. 1994. A statistical–topographic model for mapping climatological precipitation over mountainous terrain. J. Appl. Meteorol. 33:140–158.

Fan, P.F. 1979. Clays and clay minerals of hydrothermal origin in Hawaii. p. 369–374. *In* M.M. Mortland and V.C. Farmer (ed.) Developments in sedimentology. Proc. Int. Clay Conf. 6th, Oxford, UK. 10–14 July 1978. Elsevier, Amsterdam.

Fieldes, M. 1955. Clay mineralogy of New Zealand soils. Part 2. Allophane and related mineral colloids. N.Z. J. Sci. Technol. B37:326–350.

Glasmann, J.R. 1982. Alteration of andesite in wet, unstable soils of Oregon's Western Cascades. Clays Clay Miner. 30:253–263.

Hendricks, D.M., and L.D. Whittig. 1968a. Andesite weathering. I. Mineralogical transformations from andesite to saprolite. J. Soil Sci. 19:135–146.

Hendricks, D.M., and L.D. Whittig. 1968b. Andesite weathering. II. Geochemical changes from andesite to saprolite. J. Soil Sci. 19:147–153.

Jackson, M.L. 1963. Aluminum bonding in soils: A unifying principle in soil science. Soil Sci. Soc. Am. Proc. 27:1–10.

Janitzky, P. 1986. Cation exchange capacity. p. 21–23. *In* M.J. Singer and P. Janitzky (ed.) Field and laboratory procedures used in a soil chronosequence study. U.S. Geol. Surv. Bull. 1648.

Johnson, D.W., R.B. Susfalk, and R.A. Dahlgren. 1997. Nutrient fluxes in forest of the eastern Sierra Nevada mountains, United States of America. Global Biogeochem. Cycles 11:673–681.

Kirkman, J.H. 1980. Clay mineralogy of a sequence of andesitic tephra beds of western Taranaki, New Zealand. Clay Miner. 15:157–163.

Kristmannsdottir, H. 1979. Alteration of basaltic rocks by hydrothermal activity at 100–300°C. p. 359–367. *In* M.M. Mortland and V.C. Farmer (ed.) Developments in sedimentology. Proc. Int. Clay Conf., 6th, Oxford, UK. 10–14 July 1978. Elsevier, Amsterdam.

Lilienfein, J., R.G. Qualls, S.M. Uselman, and S.D. Bridgham. 2003. Soil formation and organic matter accretion in a young andesitic chronosequence at Mt. Shasta, California. Geoderma 116:249–264.

Lilienfein, J., R.G. Qualls, S.M. Uselman, and S.D. Bridgham. 2004. Adsorption of dissolved organic carbon and nitrogen in soils of a weathering chronosequence. Soil Sci. Soc. Am. J. 68:292–305.

McIntosh, P. 1979. Halloysite in a New Zealand tephra and paleosol less than 2500 years old. N.Z. J. Sci. 22:49–54.

Moore, D.M., and R.C. Reynolds. 1998. X-ray diffraction and the identification and analysis of clay minerals. Oxford Univ. Press, New York.

Mulyanto, B., G. Stoops, and E. van Ranst. 1999. Precipitation and dissolution of gibbsite during weathering of andesitic boulders in humid tropical West Java, Indonesia. Geoderma 89:287–305.

Naidu, R., J.H. Kirkman, and R.J. Morrison. 1987. Mineralogy of soils from basaltic ash, Taveuni, Fiji. Geoderma 39:181–192.

Ndayiragije, S., and B. Delvaux. 2003. Coexistence of allophane, gibbsite, kaolinite and hydroxy-Al-interlayered clay minerals in a perudic Andosol. Geoderma 117:203–214.

Nieuwenhuyse, A., and N. van Breemen. 1997. Quantitative aspects of weathering and neoformation in selected Costa Rican volcanic soils. Soil

Sci. Soc. Am. J. 61:1450–1458.
Parfitt, R.L., and C.W. Childs. 1988. Estimation of forms of Fe and Al: A review and analysis of contrasting soils by dissolution and Mossbauer methods. Aust. J. Soil Res. 26:121–144.
Parfitt, R.L., A. Parshotam, and G.J. Salt. 2002. Carbon turnover in two soils with contrasting mineralogy under long-term maize and pasture. Aust. J. Soil Res. 40:127–136.
Parfitt, R.L., M. Russell, and G.E. Orbell. 1983. Weathering sequence of soils from volcanic ash involving allophane and halloysite. Geoderma 29:41–57.
Pevear, D.R., D.P. Dethier, and D. Frank. 1982. Clay minerals in the 1980 deposits from Mount St. Helens. Clays Clay Miner. 30:241–252.
Piper, A.M., H.S. Gale, H.E. Thomas, and T.W. Robinson. 1939. Geology and groundwater hydrology of the Mokelumne area, California. U.S. Geol. Surv. Bull. 89.
Quantin, P. 1992. Les soils de l'archipel volcanique des Nouvelles-Hebrides (Vanuatu). ORSTOM, Paris.
Rasmussen, C., R.J. Southard, and W.R. Horwath. 2006. Mineral control of organic carbon mineralization in a range of temperate conifer forests. Global Change Biol. 12:834–847.
Rasmussen, C., M.S. Torn, and R.J. Southard. 2005. Mineral assemblage and aggregates control carbon dynamics in a California conifer forest. Soil Sci. Soc. Am. J. 69:1711–1712.
Reheis, M. 1999. Desert winds: Monitoring wind-related surface processes in Arizona, New Mexico and California. U.S. Geol. Surv. Prof. Pap. 1598.
Saggar, S., A. Parshotam, G.P. Sparling, C.W. Feltham, and P.B.S. Hart. 1996. C-14-labelled ryegrass turnover and residence times in soils varying in clay content and mineralogy. Soil Biol. Biochem. 28:1677–1686.
Sawhney, B.L. 1986. Electron microprobe analysis. p. 271–290. *In* A. Klute (ed.) Methods of soil analysis. Part 1.2nd ed. SSSA Book Ser. 5. SSSA, Madison, WI.
Schwertmann, U. 1985. The effect of pedogenic environments on iron oxide minerals. Adv. Soil Sci. 1:171–200.
Schwertmann, U., and R.M. Taylor. 1989. Iron oxides. p. 379–438. *In* J.B. Dixon and S.B. Weed (ed.) Minerals in soils environments. 2nd ed. SSSA Book Ser. 1. SSSA, Madison, WI
Shoji, S., M. Nanzyo, and R.A. Dahlgren. 1993. Volcanic ash soils: Genesis, properties and utilization. Dev. Soil Sci. 21. Elsevier, Amsterdam.
Singleton, P.L., M. McLeod, and H.J. Percival. 1989. Allophane and halloysite content and soil solution silicon in soils from rhyolitic volcanic material, New Zealand. Aust. J. Soil Res. 27:67–77.
Soil Survey Staff. 1996. Soil survey laboratory methods manual. Soil Surv. Invest. Rep. 42. Version 3.0. NRCS, Washington, DC.
Soil Survey Staff. 1999. Soil Taxonomy: A basic system of soil classification for making and interpreting soil surveys. NRCS, Washington, DC.
Soil Survey Staff. 2003. Keys to Soil Taxonomy. 9th ed. NRCS, Washington, DC.
Southard, R.J., and S.B. Southard. 1987. Sand-sized kaolinized feldspar pseudomorphs in a California Humult. Soil Sci. Soc. Am. J. 51:1666–1672.
Southard, S.B., and R.J. Southard. 1989. Mineralogy and classification of andic soils in northeastern California. Soil Sci. Soc. Am. J. 53:1784–1791.
Stumm, W. 1992. Chemistry of the solid–water interface. John Wiley & Sons, New York.
Takahashi, T., R.A. Dahlgren, B.K.G. Theng, J.S. Whitton, and M. Soma. 2001. Potassium-selective, halloysite-rich soils in volcanic materials from northern California. Soil Sci. Soc. Am. J. 65:516–526.
Takahashi, T., R.A. Dahlgren, and P. Van Susteren. 1993. Clay mineralogy and chemistry of soils formed in volcanic materials in the xeric moisture regime of northern California. Geoderma 59:131–150.
Talibudeen, O. 1981. Precipitation. p. 81–114. *In* D.J. Greenland and M.H.B. Hayes (ed.) The chemistry of soil processes. John Wiley & Sons, New York.
Wada, K. 1989. Allophane and imogolite. p. 1051–1087. *In* J.B. Dixon and S.B. Weed (ed.) Minerals in soils environments. 2nd ed. SSSA Book Ser. 1. SSSA, Madison, WI.
Weaver, R.M., J.K. Syers, and M.L. Jackson. 1968. Determination of silica in citrate–bicarbonate–dithionite extracts of soils. Soil Sci. Soc. Am. Proc. 32:497–501.
Whittig, L.D., and W.R. Allardice. 1986. X-ray diffraction techniques. p. 331–362. *In* A. Klute (ed.) Methods of soil analysis. Part 1. 2nd ed. SSSA Book Ser. 5. SSSA, Madison, WI.
Wood, S.H. 1977. Distribution, correlation, and radiocarbon dating of late Holocene tephra, Mono and Inyo Craters, eastern California. Geol. Soc. Am. Bull. 88:89–95.
Yuan, G., B.K.G. Theng, R.L. Parfitt, and H.J. Percival. 2000. Interactions of allophane with humic acid and cations. Eur. J. Soil Sci. 51:35–41.
Zehetner, F., W.P. Miller, and L.T. West. 2003. Pedogenesis of volcanic ash soils in Andean Ecuador. Soil Sci. Soc. Am. J. 67:1797–1809.